Available online at www.sciencedirect.com
ScienceDirect
Journal of Nuclear Materials 372 (2008) 293–303
journal of nuclear materials
www.elsevier.com/locate/jnucmat

Stress-corrosion crack initiation and propagation behavior of Zircaloy-4 cladding under an iodine environment

Sang Yoon Park *, Jun Hwan Kim, Myoung Ho Lee, Yong Hwan Jeong

Advanced Core Materials Laboratory, Korea Atomic Energy Research Institute, 150 Doekjin-dong, Yuseong-gu, Daejeon 305-353, Republic of Korea

Received 12 July 2006; accepted 6 March 2007

Abstract

Iodine-induced stress-corrosion cracking (ISCC) properties and the associated ISCC process of Zircaloy-4 fuel cladding were evaluated. Cladding was heat-treated to have either stress-relieved (SR) or recrystallized (RX) microstructures, and then an internal pressurization with a smooth and pre-cracked specimen was performed at 350 °C, in an iodine environment. The results showed that the threshold stress-intensity factor (K_{ISCC}) of the SR and RX Zircaloy-4 claddings were 3.3 and 4.8 MPa $m^{0.5}$, respectively. The crack propagation rate of the RX Zircaloy-4 was 10 times lower than that of the SR one. Crack initiation and propagation mechanisms of Zircaloy-4 claddings, which had different microstructures, were proposed by a grain-boundary pitting model and a pitting-assisted slip cleavage model; they showed reasonable results.

1. Introduction

Since 1970, it has been reported that a pellet-cladding interaction (PCI) mainly governs the failure of a fuel rod in a light water reactor (LWR) [1–3]. PCI occurs when both a chemical reaction and a mechanical contact inside a cladding simultaneously, which results in failure of a fuel rod caused by a stress-corrosion cracking (SCC). One of the causative agents of SCC is known to be gaseous iodine, which is generated between the grain boundaries of the uranium dioxide during the fission reaction, hence called an iodine-induced stress-corrosion cracking (ISCC). When the power of a LWR is frequently being changed such as in load following operation, the possibility of releasing a fission-product gas will be so large that the tendency for SCC will be increased. Nowadays, most of the nuclear power reactors are adopting a high burn-up operation to increase the fuel economy, where the refueling cycle of the fuel bundles is extended. As the fuel burn-up proceeds, the diameter of the cladding is decreased, whereas the outer diameter of the fuel pellet is increased, so that the pellet and the cladding contact each other. Also, the concentration of the iodine inside the fuel rod gradually increases so that the possibility of both mechanical and chemical interaction, which causes SCC, is increased [3–7].

As many kinds of high burn-up fuel claddings have been developed, a number of researches have focused on the investigation of the ISCC characteristics of PWR fuel cladding [8]. Lemaignan and Schuster [9] and Schuster et al. [10] performed ISCC experiments on a stress-relieved Zircaloy-4 cladding to evaluate the threshold stress-intensity factor (K_{ISCC}) value for commercial grade Zircaloy-4. Most of the studies have concentrated on determining the material parameters of the zirconium cladding like K_{ISCC} and the failure time (t_f) under an iodine environment, thus investigations on an initiation as well as the propagation process of an ISCC are limited at present. In addition, it has not been fully investigated why K_{ISCC} of the recrystallized Zircaloy-4 is larger than that of the stress-relieved material [11].

In this study, internal pressurization tests were conducted for smooth and pre-cracked Zircaloy-4 claddings under an iodine environment in order to investigate the ISCC

* Corresponding author. Tel.: +82 42 868 8597; fax: +82 42 862 0432.
E-mail address: nsypark@kaeri.re.kr (S.Y. Park).

0022-3115/$ - see front matter © 2007 Elsevier B.V. All rights reserved.
doi:10.1016/j.jnucmat.2007.03.258

initiation and propagation mechanisms. Fractographic observation was carried out to analyze the crack initiation and propagation process in detail. Finally, the effect of alloy heat treatment on the ISCC process was investigated.

2. Experimental procedure

2.1. Specimen preparation and pre-crack treatment

Cladding material used in this study was Zircaloy-4 cladding. It was commercially produced and supplied by Westinghouse (Ingot number: U04652P, Lot number S47-5627). Nominal dimensions and Kearns numbers of the cladding were as follows: OD = 9.5 mm, ID = 8.375 mm; $f_n = 0.655$, $f_t = 0.233$, $f_r = 0.112$. The chemical compositions are given in Table 1. As-received (AR) specimens which had a stress-relieved (SR) structure and cladding that had been heat-treated at 620 °C for 3 h to establish a fully recrystallized (RX) structure were used. Table 2 shows the test conditions used in this study. Two types of tests were performed. A time-to-rupture test, in which the cladding did not receive a pre-crack procedure, was used in order to investigate the initiation of a microcrack on a smooth surface under a corrosive environment. A pre-cracked test, where the initially pre-cracked specimen was pressurized under an iodine environment, was used to observe how an initial crack propagates. The pre-crack was made by the fatigue cracking method according to Lemaignan [12]. Cladding was cut into 130 mm lengths then a sine wave, whose displacement amplitude and frequency were 0.12 mm and 5 Hz, respectively, was applied to generate an artificial crack to a depth of 25–50% in cladding thickness. The displacement was made normally to the external surface of the claddings. Finally, it was pressurized under an iodine environment until a leak occurred, then cut into halves to conduct a microstructural observation by using an optical microscope (OM) and a scanning electron microscope (SEM). Fig. 1 shows photographs of the pre-cracked cladding after the ISCC test by OM and SEM: a pre-crack, a region of ISCC, and a ductile fracture were observed.

Table 1
Chemical composition of Zircaloy-4 cladding

Element	Weight (wt%)
Sn	1.30
Fe	0.21
Cr	0.11
Fe + Cr	0.32
C	0.012
O	0.129
Si	0.011
Zr	Balance

Table 2
Types of test

	Time-to-rupture test	Pre-crack (ISCC) test
Objective	Crack initiation	Crack propagation
Alloy	Zircaloy-4 (SR)	Zircaloy-4 (SR, RX)
Type	Smooth	Pre-cracked
Hoop stress/K_I	200–500 MPa	3–10 MPa $m^{0.5}$
Environment	With iodine	With and without iodine

2.2. ISCC test facility

An internal pressurization test was devised to simulate ISCC for a fuel cladding pressurized by high fission gas release. Maximum design pressure and temperature of the device were 90 MPa and 600 °C, respectively; each parameter could be controlled freely. To avoid inadvertent oxidation inside the cladding during the test, the inside of the cladding was treated in vacuum, followed by pressurization with high-purity argon gas. All the parameters regarding the test, such as the test temperature, pressure and test time could be monitored through a computer, as in Ref. [11].

2.3. Test procedure

Zircaloy-4 cladding was cut into 130 mm lengths for the test. As for the pre-cracked test, an artificially pre-cracked

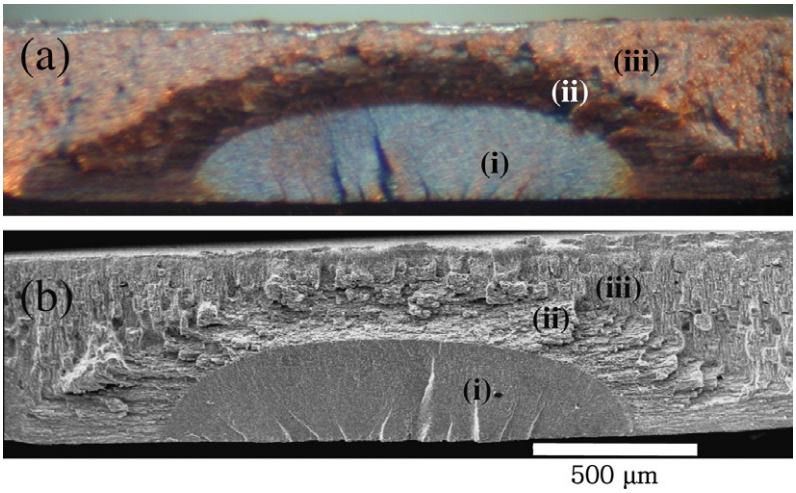

Fig. 1. Typical fracture surfaces showing (i) fatigued pre-crack, (ii) ISCC crack and (iii) ductile fracture: (a) optical microscope image and (b) SEM image.

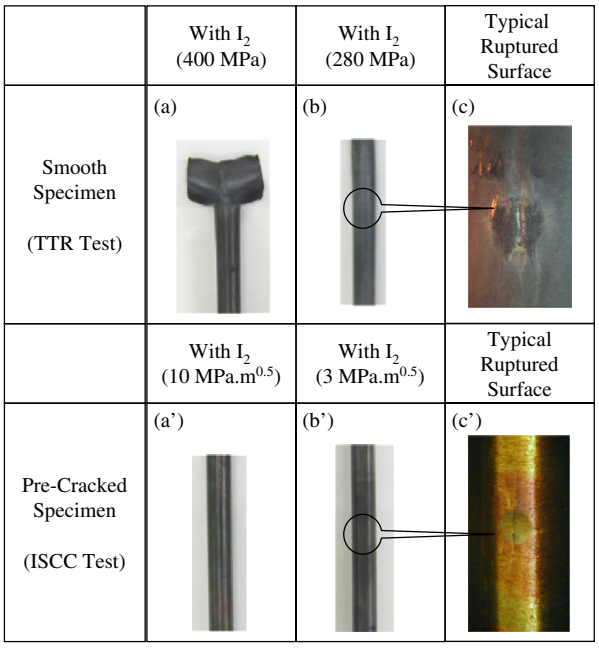

Fig. 2. Photographs of Zircaloy-4 cladding after tests and typical ruptured surfaces.

specimen was put inside the autoclave, and then the medium, which was mixed with pure argon and iodine, was pressurized inside the cladding after reaching a constant test temperature of 350 °C. The iodine used in this study, which had a purity of 99.99%, was supplied by Aldrich.

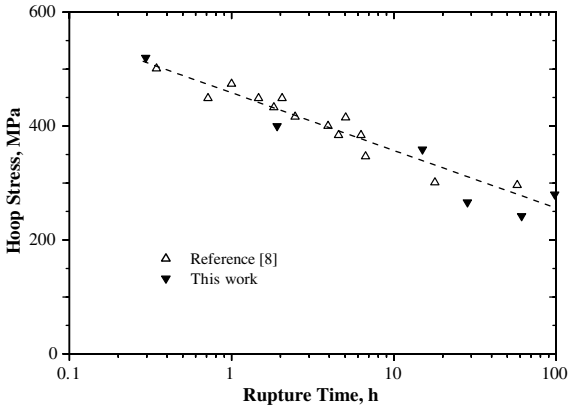

Fig. 3. Time-to-rupture behavior of Zircaloy-4 cladding in an iodine environment at 350 °C.

During the entire test period, the iodine concentration was kept constant at 1.5×10^{-3} g/cm^2. To minimize oxidation at the outer surface, the autoclave was evacuated then filled with argon gas before each test. The test was stopped either when a leakage occurred around the test specimen or, if the specimen did not leak, after reaching 100 h. After the test, the specimen was examined by using OM and SEM to determine the actual crack propagation depth during the ISCC test, and then the crack propagation velocity was evaluated. ISCC crack velocity with respect to the applied K_I was evaluated to determine the K_{ISCC} level below which no further crack propagation occurred. The K_I value was selected so that stress state round the crack

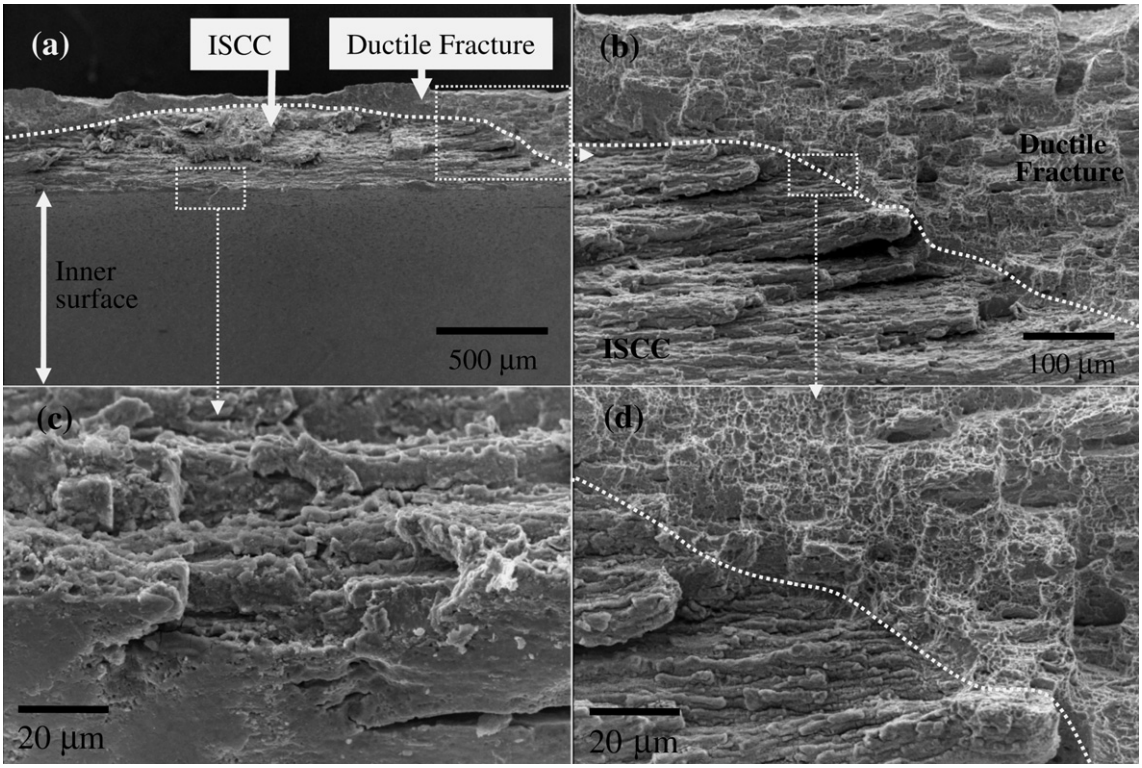

Fig. 4. Cross-section of the fracture surface at 280 MPa for 98 h (Fig. 2(b)) showing the both of ISCC and ductile fracture.

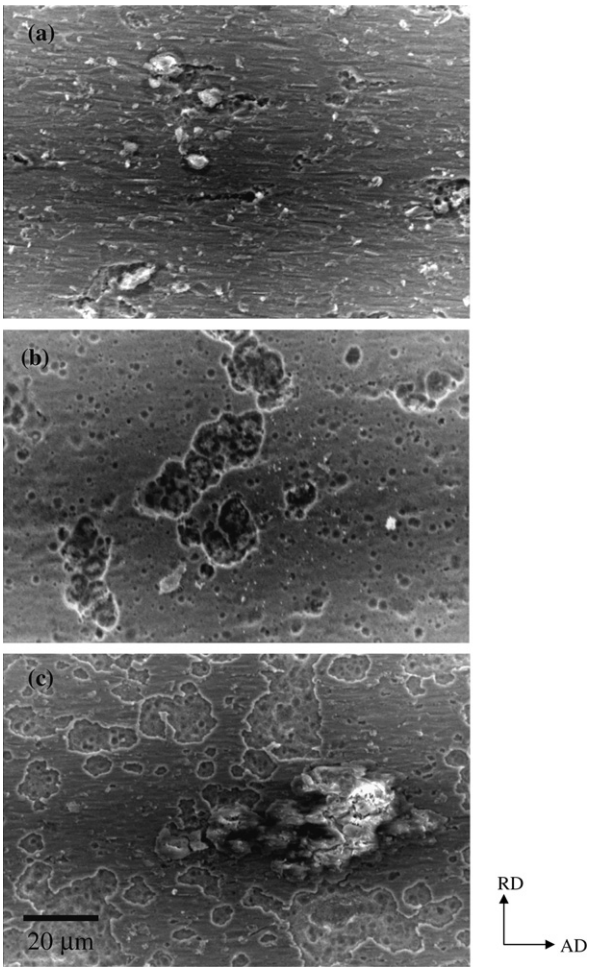

Fig. 5. SEM photographs of the inner surface after tests at 280 MPa in an iodine environments for times of (a) 1 h, (b) 50 h and (c) 98 h.

tip was a plane–strain condition according to the following relationship [13]:

$$K_I < \sigma_y (3\pi t/5)^{0.5}, \quad (1)$$

where σ_y and t, respectively, denote the yield stress and the thickness of the cladding. Thus, by considering the yield stress as 330 MPa for the SR structure at 400 °C and the thickness as 0.57 mm, the applied K_I level was limited to below 10.8 MPa $m^{0.5}$.

3. Results

3.1. Time-to-rupture test

Fig. 2 shows a photograph of the test cladding after the ISCC test. In the smooth specimen, a typical burst appearance was observed in the specimen when the applied hoop stress was above 400 MPa. At a low hoop stress, such as 280 MPa, an axial crack rather than a circumferential opening was developed for the smooth specimen, as shown in Fig. 2(b) and (c). In the pre-cracked specimen, however, a microcrack was observed at the outer surface when the applied K level was in the range of 3–10 MPa $m^{0.5}$, as seen from Fig. 2(a′)–(c′), which is assumed to be close to an actual PCI appearance where an axial crack or a pin-hole type failure are known to be the main failures observed in an actual cladding damaged by PCI [7].

Fig. 3 shows the failure time of the ruptured cladding in the iodine environments with the hoop stress. In this graph, the relationship between the time-to-rupture and the applied hoop stress can be shown by the following formula:

$$\sigma = 456 - 103.5 \times \log t, \quad (2)$$

where σ and t, respectively, mean the applied hoop stress in MPa and the rupture time in hours.

Fig. 4 shows the fractographs of a specimen after a time-to-rupture test in an iodine environment of 280 MPa for 98 h. These are the SEM pictures which were taken 50, 200 and 1000 times for the area of a crack shown in Fig. 2(c). An elliptical ISCC fractured surface is observed and dimples are also observed on the outside of the ISCC surface. They indicate a ductile fracture which was created after the time-to-rupture test.

Fig. 5 shows SEM images of the inner surface of the cladding after exposure to the iodine environment for 1 (a), 50 (b) and 98 h (c). In Fig. 5(a), several pits and a lot of small surface flaws could be observed. Average size of a flaw was 0.5 μm in width and 10 μm in length. A great number of pits with various sizes were found in Fig. 5(b) and (c). The size and number of each pit increased with the exposure time, showing that the pits which coalesced with each other to form a pitting cluster. The length of the pitting cluster gradually increased with the exposure time.

Fig. 6 shows the fractographs of a specimen after a time-to-rupture test in an iodine environment of 400 MPa for 2 h. These are the SEM pictures which were taken 100, 500, 1000 and 5000 times for the area of a crack shown in Fig. 2(a). The dimples indicate that a ductile fracture was created all over the fractured surface. Equiaxed dimples are found in an area which is far from the inner surface while elongated dimples are found in an area which is near the interface. It is observed that the dimples originated from the small pits contained in the large one.

Fig. 7 shows the SEM picture on the inner surface of a specimen which was taken from the fractured area shown in Fig. 2(a). Many pits are evolved all over the inner surface of cladding as shown in Fig. 7(a). Also, many of them are agglomerated along the axial direction and they become a microcrack. The small pits tend to coalesce into a large pit as shown in Fig. 7(c). It is observed that a fine crack evolved in the interior of a large pit.

3.2. Pre-crack test

In the stress-corrosion cracking theory, it is generally known that the crack propagation rate considerably depends on the stress-intensity factor (K_I). Kobayashi

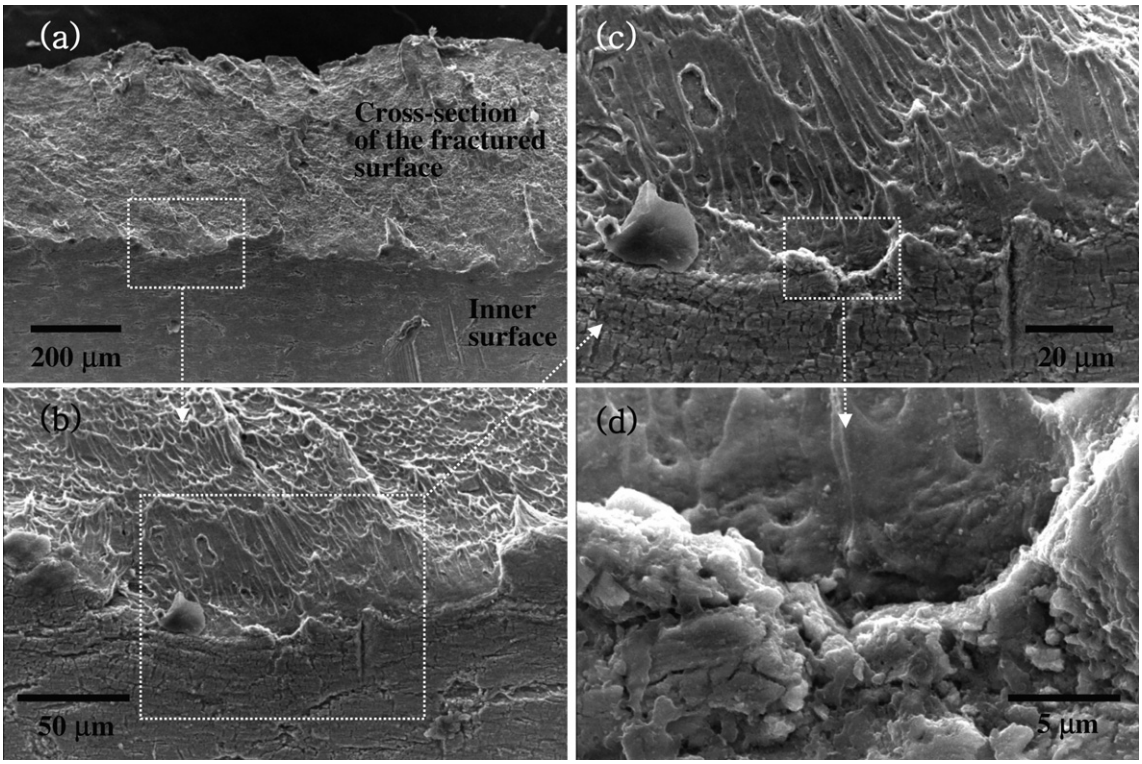

Fig. 6. Cross-section of the fractured position at 400 MPa (Fig. 2(a)) showing lots of dimples due to ductile fracture.

et al. [14] obtained a theoretical K_I formula for a thin-walled tube, and Anderson [15] improved the theoretical K_I formula by correcting the geometrical factor

$$K_I = \frac{pR}{t}\sqrt{\frac{\pi a}{Q}}F\left(\frac{a}{2c},\frac{a}{t},\frac{R}{t}\right), \tag{3}$$

where p is the internal pressure on the tube (in MPa), R the mean radius of the tube (4.465×10^{-3} m), t the tube-wall thickness (0.57×10^{-3} m), a the depth of the surface crack, Q the shape factor for an elliptical crack ($=1+1.464(a/c)^{1.65}$), c is the half-length of the surface crack and F is a boundary correction factor, which depends on the shape of the initial crack formed at the inner part of the cladding. F can be calculated by the following formula in the range of $5\leqslant R/t\leqslant 20$, $2c/a\leqslant 12$, and $a/t\leqslant 0.8$:

$$F = 1.12+0.053\xi+0.0055\xi^2 + (1+0.02\xi+0.0191\xi^2)\frac{\left(20-\frac{R}{t}\right)^2}{1400}, \tag{4}$$

where ξ denotes $(a/t)(a/2c)$. Since the R/t value of the cladding used in this study is 7.37, the above relationship can be used for the fuel cladding provided that the length of the pre-crack can be adequately controlled. The applied K_I value calculated according to the above formula was controlled such that the stress state near a crack tip is assumed to be a plane strain.

Fig. 8 shows the crack propagation rate of the Zircaloy-4 cladding in a stress-relieved condition with respect to the applied K_I value. The K_{ISCC} value of Zircaloy-4 in this study was 3.3 MPa $m^{0.5}$, which is similar to other data such as Le Boulch et al. [8] and Schuster et al. [10]. The chemical effect on the ISCC process was so large that the threshold stress intensity of the Zircaloy-4 cladding under the inert environment was increased two times and the crack propagation rate was decreased 10000 times when compared to the iodine environment.

Fig. 9 shows SEM images of the fracture surface of the Zircaloy-4 cladding after the ISCC test. Not only could the crack surface caused by the ISCC be easily identified, but also the axially elongated microstructure inside the ISCC crack which is assumed to be the stress-relieved α phase, is clearly shown.

Fig. 10 shows the crack propagation rate of Zircaloy-4 cladding having SR and RX structures. Recrystallization has increased the ISCC resistance such that the K_{ISCC} value of the SR and RX specimens are 3.3 and 4.8 MPa $m^{0.5}$, respectively; in addition, the crack propagation rate in region II has been reduced by 10 times for RX condition when compared to that of the SR condition.

Fig. 11 shows the fractographs of the RX cladding near the interface between a pre-crack and ISCC crack. Both intergranular (IG) and transgranular (TG) patterns were observed at the same time, showing that a lot of pits were developed on the IG surface. The size of the pits was less than 2 μm. Regarding the TG surface, however, a few pits were shown, to only form around the grain boundary. It can also be observed that, the main fracture

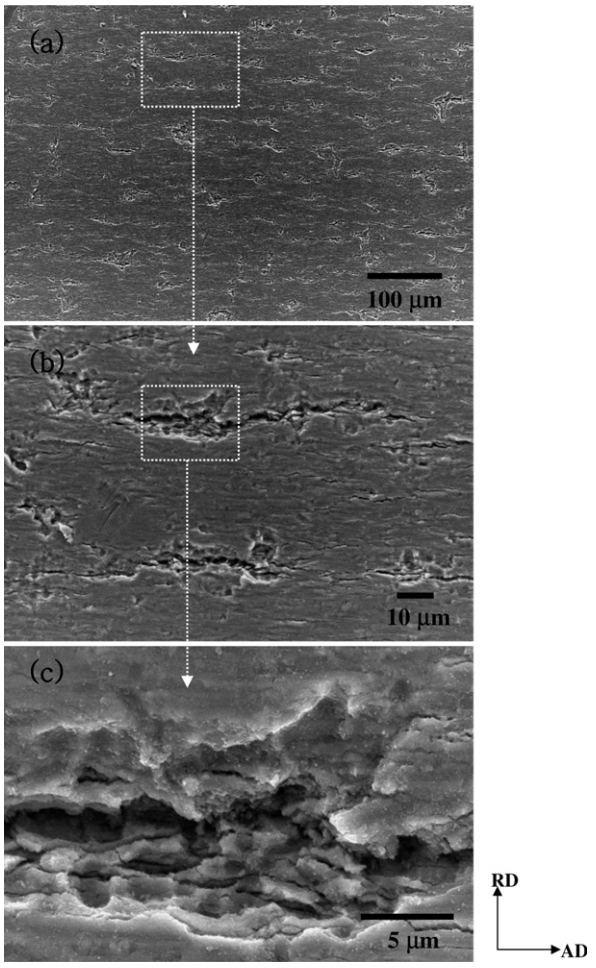

Fig. 7. Inner surface of the Zircaloy-4 cladding after test at 400 MPa (Fig. 2(a)) showing lots of pits and microcracks in the agglomerated pitting.

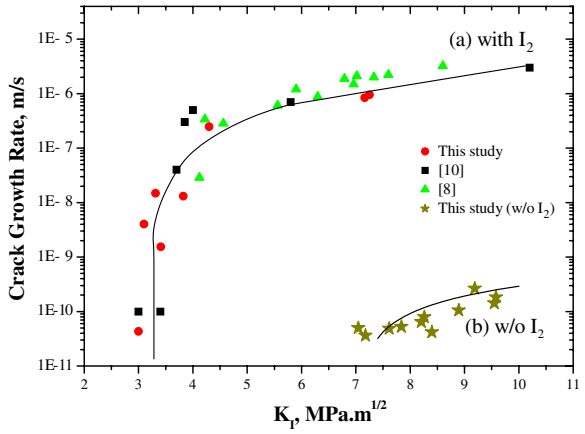

Fig. 8. Plots of da/dt vs. K_I for the SR Zircaloy-4 cladding (a) with and (b) without I_2 test.

appearance near the pre-crack and the ISCC crack interface was IG.

Fig. 12 shows the fractographs of the RX cladding near the interface between the ISCC crack and the ductile fracture. In this region, the only TG patterns according to cleavage and fluting were observed. And the pits of a μm scale which were observed in Fig. 11 were not observed. Only small and shallow pits of a nm scale were observed in the higher magnification photos (50000×).

4. Discussion

4.1. Microcrack nucleation and crack initiation

Fig. 7 shows the inner surface of cladding which was exposed to the iodine environment of 400 MPa for 2 h. In this figure, many microcracks were formed on the inner surface of the cladding. Many of the pits are gathered around the microcracks. It is seen that they coalesced into a large pitting cluster. It is understood that the corrosion is concentrated at the weak point of cladding by highly corrosive iodine and that pitting clusters play a role of nucleation sites for a crack because of the microcracks developed on the inner surface of the pitting clusters. Fig. 6 demonstrates the role of pitting clusters. The fracture in the iodine environment of 400 MPa is a ductile fracture because dimples are developed all over the fractured surface. These dimples originate from a second pit in a pitting cluster which is located at the interface between the inner and fractured surface of the cladding. It is an equiaxed type far from an interface but an elongated one near an interface. The dimples are facing the pitting cluster. In other words, it is understood that a pitting cluster plays a role of a nucleation site for a crack.

Figs. 4 and 5 show the morphologies of the fractured and the inner surface of the cladding which was exposed to the iodine environment of 280 MPa for 98 h. Fig. 6 shows dimples on the ductile fractured surface when the cladding was exposed to an iodine environment of 400 MPa for short time while Fig. 4 shows a brittle cleavage with ISCC on the fractured surface when the cladding was exposed to an iodine environment of 280 MPa for a long time. The ISCC fractured surface in Fig. 4 is the same morphology that Le Boulch et al. [8], Lemaignan and Schuster [9], and Schuster et al. [10] reported. Fig. 4(c) also shows that ISCC crack initiated from the pitting cluster on the inner surface of the cladding. The pitting cluster increases with time as shown in Fig. 5. It could play a role of a crack nucleation site under a high stress concentration due to the increased internal pressure.

Williford [16] has reported that the ISCC process for Zircaloy-4 cladding can be divided into (1) a microcrack nucleation, (2) a crack initiation, (3) a crack growth and (4) a cladding rupture. In terms of the microcrack nucleation, he remarked that a pre-existing flaw and a damaged region mainly affected the crack nucleation, rather than grain-boundary attack and pitting.

Fig. 5(b) shows the fracture surface exposed for 50 h. From this figure, pits do not preferentially initiate around the microflaw; instead, they are randomly distributed over the surface. In, Fig. 11, pits are preferentially generated

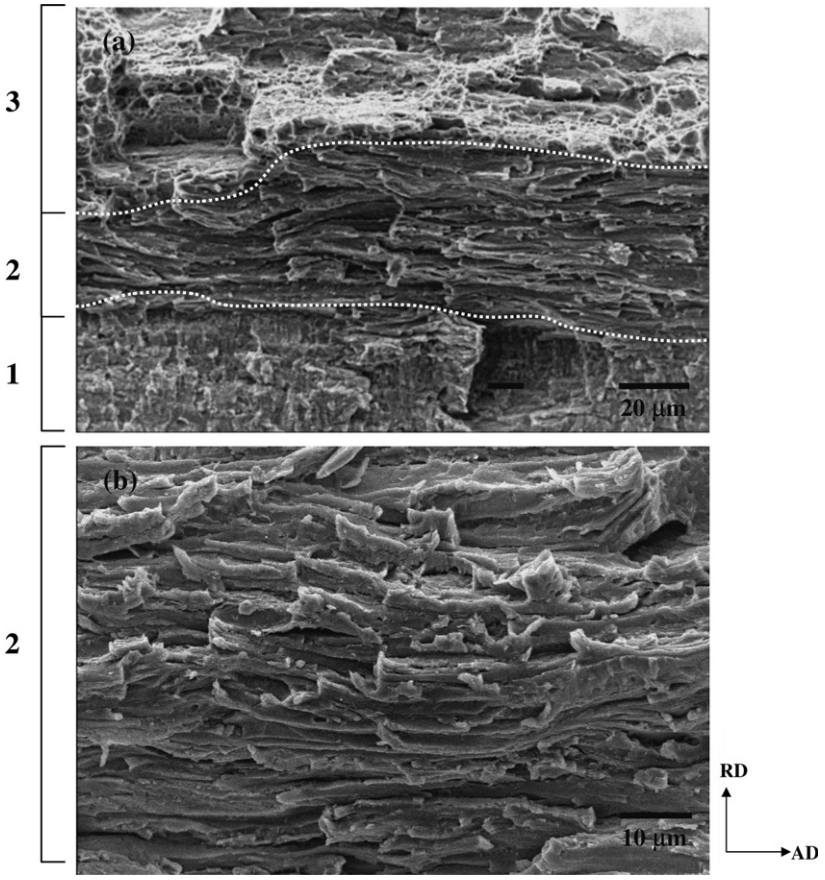

Fig. 9. Fracture surface of Zircaloy-4 (SR) pressurized in an iodine environment at 350 °C: (1) fatigue pre-crack, (2) SCC and (3) dimple by tensile fracture.

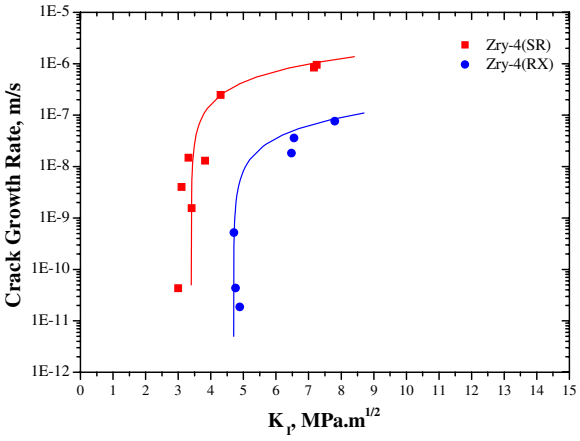

Fig. 10. Plots of da/dt vs. K_I for the (a) SR and (b) RX Zircaloy-4 claddings.

along the grain boundary, rather than inside the grain. Such trends were consistent along the crack surface, regardless of the iodine exposure time.

In short, although small flaws are generated on the inner surface of the cladding under the iodine environment, they may not develop into pits if the flaws are located inside the grain. On the other hand, pits are likely to grow on the surface around the grain boundary when it is exposed to an iodine environment even if there are no flaws. As the grains are elongated along the axial direction in the case of the SR microstructure, their long grain boundaries are easily attacked by the iodine to become a macrocrack site.

When the iodine is adsorbed into the zirconium cladding, the zirconium bond at the grain boundary (GB) will be weakened, so the surface energy will be reduced [17,18]. In addition, the free iodine can react with zirconium to form solid iodides and a gaseous zirconium tetra-iodide (ZrI_4) [19]. This gaseous ZrI_4 can be decomposed easily into the iodine at a strained surface by an applied hoop stress, thus pits are formed due to a localized attack on the GB. There are two aspects regarding the preferential attack around the GB. First, the GB will be embrittled locally because it has a large amount of impurities such Fe, Al, Si and Cr [19]. Second, if a sufficient hoop stress is applied to the surface then a slip band will be formed around the GB surface thus increasing the instability [20,21]. These aspects support our results as why the pitting preferentially nucleates, grows and coalescences around the GB. Such a crack initiation process may be governed by a grain-boundary pitting coalescence (GBPC). From the standpoint of the GBPC, crack initiation is not influenced by a microflaw inside the cladding, which is inevitably

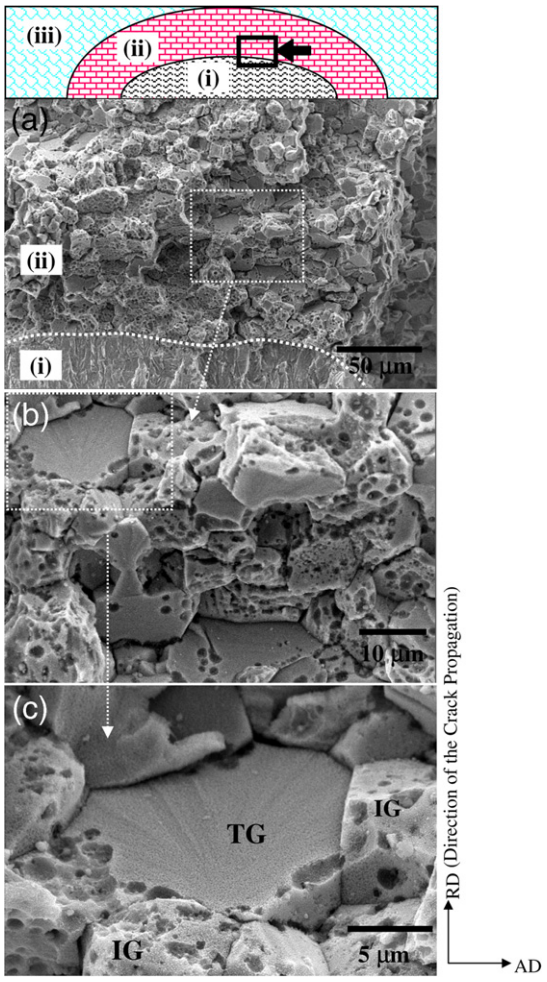

Fig. 11. Fractographs of the RX cladding near the interface between a pre-crack and an ISCC crack pressurized in an iodine environment at 350 °C showing transgranular (TG) and intergranular (IG) fracture: (i) fatigued pre-crack, (ii) ISCC and (iii) ductile fracture after test.

generated during the manufacturing process, but by the grain size, shape and orientation which are mainly affected by the heat-treatment process.

Knorr et al. [22] and Cubicciotti et al. [23] observed lots of pitting on the inner surface of the Zircaloy cladding after ISCC test, and Videm and Lunde [24] reported on an IG pitting attack which appeared more and more crack-like as the attack penetrated into the metal. But they did not concentrate on the effect of pitting on a crack initiation and propagation.

4.2. Crack propagation

It has been reported that ISCC cracks proceed along the grain boundaries at the initial stage, and then propagate across the grains to leave a fracture pattern as a cleavage during the ISCC process [7]. Although Le Boulch et al. [8] have postulated crack propagation in fuel cladding under PCI when the hoop stress caused by an expansion of a fuel pellet and corrosion by iodine occur simultaneously, the mechanism related to the crack propagation has not been demonstrated at present.

The morphology of an ISCC fractured surface (Fig. 9) on the SR structure cladding in this study was consistent with that from the other studies [8–10]. The TG cracking in the SR structure of cladding propagated as a kind of pseudo-cleavage by a fluting or tearing as Shimada and Nagai [25] suggested. However, the fractured surface on the RX structure cladding at the initial cracking is quite different from that shown in Fig. 11. It shows a mixture of IG and TG crack. Many dimples are found at the interface between IG and TG fractured surface. The distinctive feature of an initial fractured surface of RX structure could be summarized as follows:

(1) A few transgranular cracks occur along with lots of intergranular cracks along the crack direction.
(2) A cleavage crack that passed through one grain cannot penetrate further into the neighboring grain so soon, it changes direction along the grain boundary to show an intergranular crack along several grains. After some intergranular cracks have proceeded, then a transgranular crack occurs. Such a process is repeated during the ISCC process.
(3) A lot of pits are generated on the cracks that propagated along the grain boundary. Their size and density increased as the exposed time increased.
(4) Pits are generated not inside the transgranular crack, but along the grain boundaries.

From the above summary, the GBPC mechanism, mentioned in the previous paragraph, affects not only a crack initiation but also a crack propagation of the ISCC process in the zirconium cladding.

The TG cracking in the center of Fig. 11(c) shows a cleavage surface. It is interesting that the pits and their clusters are developed only at the bottom side of the GB. It is understood that a cleavage crack was triggered at the bottom side of the GB because the stress had been concentrated there by the arrangement of the pits with their clusters. The mechanism of the TG cracking might be the same as that of the inner surface cracking on the cladding which is shown in Fig. 7(c).

Both a crack nucleation at the inner surface of cladding and a cleavage crack nucleation at a grain boundary of the RX structure would be caused by a pitting coalescence. It is generally known that a TG crack in Zircaloy would propagate in parallel to a basal plane [7,17,26–28]. But Peehs et al. [29] reported that the crack would propagate easily in the 50–70° direction to a basal plane. Cox [7] also reported that a TG crack would propagate along a slippery prism plane as well as a basal plane.

Zircaloy cladding of a commercial grade would be manufactured with the normal to a basal pole along the radial direction because the basal plane tends to be a habit plane for a hydride. The f_n index of the cladding specimen used in this study was 0.655. The ISCC in the cladding would

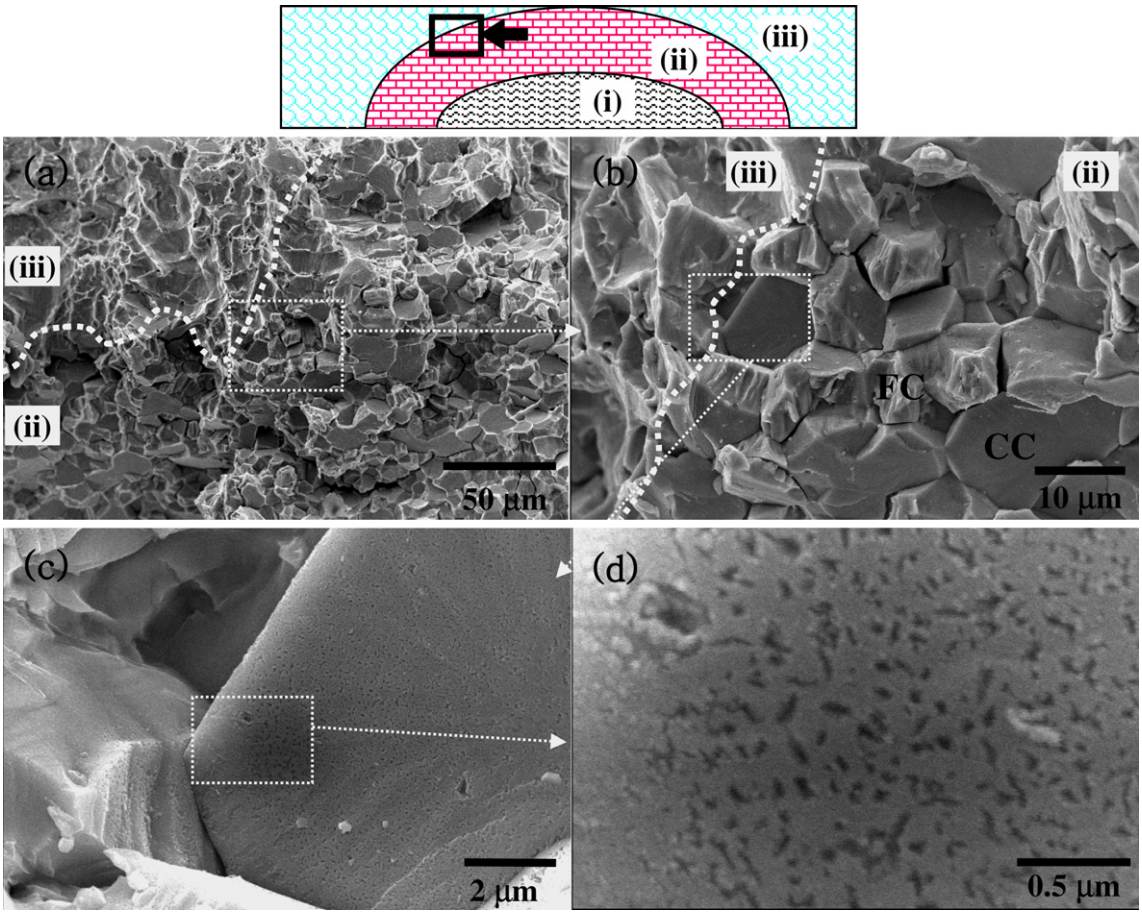

Fig. 12. Fractographs of the RX cladding near the interface between the ISCC fracture and the ductile fracture pressurized in an iodine environment at 350 °C showing cleavage cracking (CC) and fluting cracking (FC) fracture: (i) fatigued pre-crack, (ii) ISCC and (iii) ductile fracture after test.

propagate easily along radial direction of cladding on the prism plane. If an active crystal slip encounters a grain boundary, the grain boundary will be attacked and pitted easily by iodine because it becomes weaker. If the pitting clusters at the bottom of grain boundary get into the slip system and trigger a cleavage on the fractured surface, it could be named as a pitting-assisted slip cleavage (PASC).

Fig. 12 shows the interface on the final phase of ISCC propagation between the ISCC fractured surface and the ductile fractured surface. In this figure, the cracking mode was almost TG due to fluting, tearing or cleavage but it shows very few pits of a μm scale which were found on the IG cracked surface in Fig. 11. However, well distributed fine pits of a nm scale can be seen in the 50 000× SEM picture for the same region in Fig. 12. As the depth of crack becomes deeper, the stress is concentrated on the crack tip. Thus, it seems that the PASC mechanism can be activated even at a small pitting of a nm scale. In the SR structure, a TG crack tends to propagate because the grains are elongated along the axial direction and laminated thinly along the radial direction. So, the PASC mechanism could be actuated in a SR structure without pits of a μm scale. But the fine pits of a nm scale could not be observed in the SR structure because many of the grains were twisted.

Since such GBPC and PASC mechanisms can be activated due to the corrosive characteristics of iodine, the effect of iodine on the crack rate was very severe, as shown in Fig. 8. Thus, the propagation rate of the crack in the iodine environment was 10 000 times faster than that in the inert environment and the K_{ISCC} was also decreased to below one half.

In general, intergranular cracking in an inert environment is mainly generated by successive events, such as a microvoid nucleation, microvoid coalescence, grain-boundary crack, cavity formation and decohesion [16]. In the case of an iodine environment, however, many pits are generated around the GB, showing intergranular and transgranular fractures, which are mixed along the crack length. A crack was quickly initiated by the GBPC to reach a lower K_{ISCC} value than the microvoid alone. Grain-boundary attacks by pits are continuously being developed to achieve a higher crack propagation rate. In summary, an intergranular attack caused by a GBPC as well as a transgranular cleavage caused by a PASC occur at the same time to increase the crack propagation rate of Zircaloy-4 cladding under an iodine environment much more so than that

under an inert one, where the crack propagation process is governed only by the microvoid nucleation and its associated coalescences. Thus, the increase of the crack propagation rate by iodine is 10000 times higher than that by the inert environment, as shown in Fig. 8.

4.3. Effect of the microstructure

As shown in Figs. 9 and 11, stress-relieved (SR) microstructure has a laminar grain structure, which is elongated along the axial direction, whereas the recrystallized (RX) microstructure has an equiaxed one. Thus, when the cladding is exposed to an iodine environment, an axially elongated crack will be generated inside the cladding with an SR microstructure, whereas an equiaxed microcrack will be generated inside the cladding with an RX microstructure.

Fig. 13 shows the schematic illustrations for the microcrack nucleation in the cladding that has either SR or RX microstructure, where it is easily seen that the possibility of generating an axial microcrack will increase for the SR microstructure. The grain size of the SR microstructure was 25 μm in length in the axial direction and 3 μm in height in the radial direction, whereas, that of the RX microstructure was 6 μm equiaxed. As the grains in the SR microstructure are elongated, the exposed grain-boundary line will be increased when compared to the RX structure.

Many cracks were observed along the axial direction in Fig. 7 which shows the initial cracks that were developed in the inner surface of the SR structure cladding. They were found to be as the initial cracks that had originated from the coalescence of the pits along the grain boundaries. The initial cracks would propagate until the stress reached the value of K_{ISCC} with an activation of the GBPC mechanism. An initial crack could be created easily and the K_{ISCC} could be lowered in the SR structure because long grain boundaries are exposed to the inner surface of the cladding. As reported in Table 3, K_{ISCC} values of the SR and RX claddings were, respectively, 3.2–3.4 and 4.8 MPa $m^{0.5}$, which verifies that the resistance of the ISCC decreased in the SR condition.

In Fig. 10, it was revealed that the crack propagation rate in region II of the SR microstructure was 10 times higher than that of the RX microstructure. In the early stage of a crack propagation of the RX heat-treated cladding (Fig. 11), an intergranular fracture by a GBPC and transgranular fracture by a PASC occurred simultaneously during the cracking process, resulting in islands of transgranular fractures among lots of the intergranular fractures. In the SR heat-treated cladding, on the other hand, transgranular fractures are mainly found from the beginning of the crack propagation as shown in Fig. 9. Since the grain shape of the SR structure is a laminar type, which is elongated along the axial direction, the nm scale pits can initiate a transgranular crack on the SR cladding, and the tendency for the occurrence of transgranular cracking will be higher than that for the RX cladding. Thus, the higher possibilities of the PASC may lead to a higher crack propagation rate for the SR cladding.

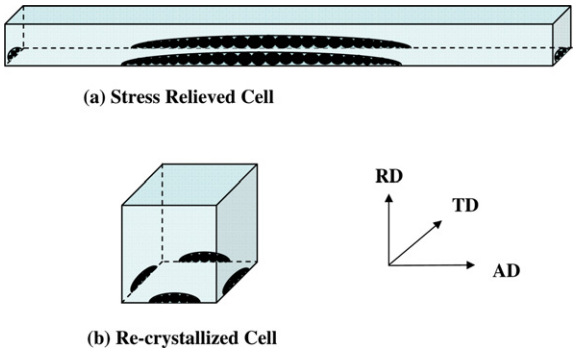

Fig. 13. Schematic diagrams of the crack initiation by agglomerated pitting on the inner surface of (a) SR and (b) RX Zircaloy-4 cladding.

Table 3
Threshold stress-intensity factor for the Zircaloy-4 claddings at 350 °C

Alloy	Microstructure	K_{ISCC}	Reference
Zircaloy-4	SR	3.4	[9]
	SR	3.2	[10]
	SR	3.3	This work
	RX	4.8	This work

5. Conclusions

Time-to-rupture tests and associated crack propagation tests under an iodine environment were performed on Zircaloy-4 cladding with either SR or RX microstructures to investigate the ISCC process and the following can be summarized:

1. When Zircaloy-4 cladding is exposed to a high-temperature, high-pressure iodine environment, pits will generate preferentially around the grain boundaries. They will coalescence with each other to form a microcrack to accommodate a site for a crack initiation. (grain-boundary pitting coalescence, GBPC model) The microcrack may develop into an incipient crack that initiates and propagates along the grain boundary. This incipient crack is more evident for SR structure than RX structure because of the grain morphology.
2. From fractographic observation, lots of pits were generated on the IG crack surface. When they were combined into the crystallographic slip plane, a cleavage crack was generated to a certain extent (pitting-assisted slip cleavage, PASC model).
3. The chemical effect of iodine from the point of view of the GBPC and PASC models on the crack propagation was very high, that is, the crack velocity was increased by 10000 times and the K_{ISCC} was decreased by 1/2 times than those of the inert environment.

4. The ISCC resistance of the cladding with a recrystallized structure increased in that the K_{ISCC} value of the stress-relieved and recrystallized Zircaloy-4 was, respectively, 3.2–3.4 and 4.8 MPa $m^{0.5}$, as well as the crack propagation rate which was reduced by 10 times. This can be explained quite well in terms of the GBPC and PASC models.

Acknowledgement

The work reported in this paper has been carried out under the Nuclear R&D program by MOST.

References

[1] M.F. Lyons, D.H. Coplin, G.G Jones, High performance UO_2 fuel program, GEAP-3771-10,11,12, 1963/1964.
[2] H.S. Rosenbaurm, Electrochem. Technol. 4 (1966) 153.
[3] J.A.L. Robertson, in: Proceedings of the Joint Topical Meeting on Commercial Nuclear Fuel Technology Today, Toronto, April 1975, CNS-ISSN-0068-8517.
[4] F. Garzarolli, R. von Jan, H. Stehle, At. Energy Rev. 17 (1979) 31.
[5] J.C. Wood, J.R. Kelm, Res. Mech. 8 (1983) 127.
[6] J.C. Wood, Nucl. Technol. 23 (1974) 63.
[7] B. Cox, J. Nucl. Mater. 172 (1990) 249.
[8] D. Le Boulch, L. Fournier, C.S. Catherine, in: International Seminar on Pellet-Cladding Interaction in Water Reactor Fuels, held in March 2004, Aix en Provence, France.
[9] C. Lemaignan, I. Schuster, in: Proceedings of the Technical Committee Meeting on Properties of Materials for Water Reactor Elements and Methods of Measurement, Vienna, Austria, 13–16 October 1986.
[10] I. Schuster, C. Lemaignan, J. Joseph, SMiRT-12C03/2, 1993, p. 45.
[11] L. Brunisholz, C. Lemaignan, in: Proceedings of the Seventh International Conference on Zirconium in Nuclear Industry, ASTM-STP 939, 1985, p. 700.
[12] C. Lemaignan, Int. J. Pres. Ves. Pip. 15 (1984) 241.
[13] Yu.K. Bibilashvily, Yu.N. Dolgov, B.I. Nesterov, V.V. Novikov, J. Nucl. Mater. 224 (1995) 307.
[14] A.S. Kobayashi, N. Polvanich, A.F. Emery, W.J. Love, J. Press. Ves. Technol., Trans. ASME (February) (1977).
[15] T.L. Anderson, Fracture Mechanics – Fundamentals and Applications, 2nd Ed., CRC Press, 1995, p. 636.
[16] R.E. Williford, J. Nucl. Mater. 132 (1985) 52.
[17] J.C. Wood, J. Nucl. Mater. 45 (1972) 105.
[18] B. Cox, J. Nucl. Mater. 170 (1990) 1.
[19] D. Cubicciotti, R.L. Jones, B.C. Syrett, in: Zirconium in the Nuclear Industry, Boston, MA, ASTM STP 754, 1982, p. 146.
[20] T. Kubo, Y. Wakashima, K. Amano, M. Nagai, J. Nucl. Mater. 132 (1985) 1.
[21] P. Jacques, F. Lefbvre, C. Lemaignan, J. Nucl. Mater. 264 (1999) 239.
[22] D.B. Knorr, J.M. Peltier, R.M. Pelloux, in: Zirconium in the Nuclear Industry, Vancouver, BC, ASTM STP 824, 1984, p. 627.
[23] D. Cubicciotti, R.L. Jones, B.C. Syrett, Stress corrosion cracking of Zircaloys, EPRI NP-1329, 1980, p. A.7.
[24] K. Videm, L. Lunde, in: ANS Topical Meeting on Water Reactor Fuel Performance, Charles, IL, 1977, p. 274.
[25] S. Shimada, M. Nagai, J. Nucl. Mater. 114 (1983) 222.
[26] R.L. Jones, D. Cubicciotti, B.C. Syrett, J. Nucl. Mater. 91 (1980) 277.
[27] B.C. Syrett, D. Cubicciotti, R.L. Jones, Nucl. Technol. 55 (1981) 628.
[28] R.B. Adamson, J. Nucl. Mater. 82 (1980) 363.
[29] M. Peehs, H. Stehle, E. Steinberg, in: Proceedings of the Fourth International Symposium on Zirconium in the Nuclear Industry, Stratford-upon-Avon, England, June 1978, ASTM STP-681, p. 244.